Chinese Chemical Letters xxx (2019) xxx–xxx

Contents lists available at ScienceDirect

Chinese Chemical Letters

journal homepage: www.elsevier.com/locate/cclet

Communication

Bulk heterojunction perovskite solar cells incorporated with solution-processed TiO_X nanoparticles as the electron acceptors

Tao Zhu[a,1], Yongrui Yang[a,1], Suyuan Zhou[a], Xiang Yao[b], Lei Liu[a], Wenping Hu[b,*], Xiong Gong[a,*]

[a] Department of Polymer Engineering, College of Polymer Science and Polymer Engineering, The University of Akron, Akron, OH 44325, United States
[b] Institute of Molecular Plus, Tianjin Key Laboratory of Molecular Optoelectronic Sciences, School of Science, Tianjin University and Collaborative Innovation Centre of Chemical Science and Engineering, Tianjin 300072, China

ARTICLE INFO

Article history:
Received 29 December 2019
Received in revised form 24 January 2020
Accepted 5 February 2020
Available online xxx

Keywords:
Bulk heterojunction
Perovskite
TiO_X
Balanced mobilities
Stability

ABSTRACT

In the past ten years, perovskite solar cells were rapidly developed, but the intrinsic unbalanced charge carrier diffusion lengths within perovskite materials were not fully addressed by either a planar heterojunction or meso-superstructured perovskite solar cells. In this study, we report bulk heterojunction perovskite solar cells, where perovskite materials $CH_3NH_3PbI_3$ is blended with solution-processed n-type TiO_x nanoparticles as the photoactive layer. Studies indicate that one-step solution-processed $CH_3NH_3PbI_3$:TiO_x bulk-heterojunction thin film possesses enhanced and balanced charge carrier mobilities, superior film morphology with enlarged crystal sizes, and suppressed trap-induced charge recombination. Thus, bulk heterojunction perovskite solar cells by $CH_3NH_3PbI_3$ mixed with 5 wt% of TiO_X, which is processed by one-step method rather than typical two-step method, show a short-circuit current density of 20.93 mA/cm^2, an open-circuit voltage of 0.90 V, a fill factor of 80% and with a corresponding power conversion efficiency of 14.91%, which is more than 30% enhancement as compared with that of perovskite solar cells with a planar heterojunction device structure. Moreover, bulk heterojunction perovskite solar cells possess enhanced device stability. All these results demonstrate that perovskite solar cells with a bulk heterojunction device structure are one of apparent approaches to boost device performance.

Since perovskite solar cells (PSCs) with a power conversion efficiency (PCE) of 3.8% were first reported by Miyasaka and his co-workers [1], PSCs have been drawn great attention in both academic and industrial sectors in the past ten years [2–5]. Over 25% PCE was reported by Korea Research Institute of Chemical Technology collaborated with Massachusetts Institute of Technology [6]. However, the intrinsic electronic properties, *i.e.*, the diffusion length of the hole is greater than that of the electron ($L_{eff,\ h^+}/L_{eff,\ e^-} > 1$), of hybrid perovskite, which restricted further boosting device performance of PSCs, was not fully addressed so far [7]. In order to balance charge carrier transporting, high-temperature sintered TiO_X (or Al_2O_3) electron extraction layer (EEL) was used as the scaffold in the meso-superstructured PSCs, which was similar to that of dye sensitized solar cells [8–13]. On the other hand, fullerene or fullerene derivatives used as the EEL in PSCs with a planar heterojunction (PHJ) device structure to enhance the extraction of electrons to the cathode [14]. But the electrical conductivities of above EELs are still not good enough to enhance the separated electrons to be transported and then eventually be collected, thus PCEs of PSCs were still poor [15]. Towards the end, we reported PSCs with a bulk heterojunction (BHJ) device structure, where perovskite materials were mixed with n-type electron acceptors, for balancing charge carrier transport properties, and then boosting PCEs of PSCs [15,16].

Based on our previous report on BHJ PSCs [15–18], we report BHJ PSCs in this study, where perovskite materials $CH_3NH_3PbI_3$ is mixed with solution-processed n-type TiO_x nanoparticles rather than organic molecules. Solution-processed n-type TiO_x nanoparticles are selected as the electron acceptors since it possesses high electron mobility and has a good solubility in the solvent which is used for dissolving $CH_3NH_3PbI_3$. It is found that $CH_3NH_3PbI_3$:TiO_x BHJ thin film possesses enhanced and balanced charge carrier mobilities, superior film morphology with enlarged crystal sizes, and suppressed trap-induced charge recombination. Thus, BHJ PSCs exhibit more than 30% enhancement in PCEs as

* Corresponding authors.
E-mail addresses: huwp@tju.edu.cn (W. Hu), xgong@uakron.edu (X. Gong).
[1] These authors contributed equally to this work.

https://doi.org/10.1016/j.cclet.2020.02.004
1001-8417/

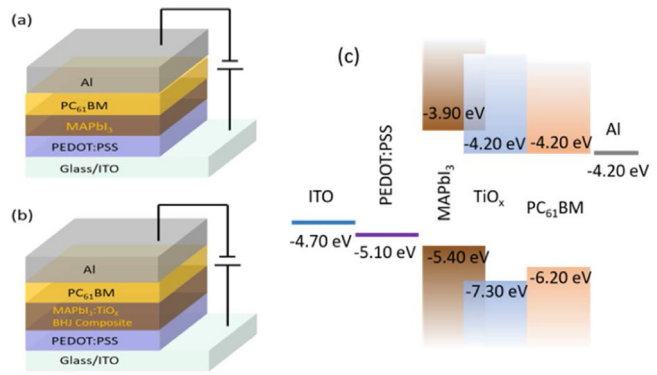

Scheme 1. Device structures of perovskite solar cells with (a) a planer heterojunction and (b) bulk heterojunction device structures. (c) The LUMO and HOMO energy levels of CH3NH3PbI3 (MAPbI3), TiOX and PC61BM and the work functions of ITO, PEDOT:PSS and Al, respectively.

compared with that of PHJ PSCs. In addition, BHJ PSCs possess enhanced device stability.

Poly(3,4-ethylene dioxy-thiophene):poly(styrene sulfonate) (PEDOT:PSS, SCA 388-20) was purchased from Heraeus. Lead iodide (PbI_2, 99.99.5% metals basis) was purchased from Alfa Aesar. Phenyl-C61-butyric acid methyl ester ($PC_{61}BM$, 99.5%) was purchased from Solenne BV. Dimethylformamide (DMF, anhydrous, 99.8%), dimethyl sulfoxide (DMSO, anhydrous, 99.9%), toluene (anhydrous, 99.8%), and chlorobenzene (anhydrous, 99.8%) were purchased from Sigma-Aldrich. All materials are used as received without any further processing. Methyl-ammonium iodide (MAI, CH_3NH_3I) was synthesized in our laboratory [19–22].

Perovskite precursor solution was prepared by dissolving PbI_2 and MAI (molar ratio of 1:1) into DMF:DMSO (volume ratio of 4:1) with the concentration of 1 mol/L. TiO_X precursor solution was prepared by diluting tetrabutyl titanate (TBT) with isopropyl alcohol solution (concentration of 3 vol%). $PC_{61}BM$ was dissolved in chlorobenzene with a concentration of 20 mg/mL.

The pre-cleaned indium tin oxide (ITO)/glass substrates were treated by UV-ozone plasma for about 20 min. Then, a ~ 40 nm PEDOT:PSS thin film was spin-cast on the top of the substrates with a spin speed of 3500 rpm for 30 s, followed with thermal annealing at 150 °C for 10 min. After PEDOT:PSS coated substrates are cooled down to room temperature, and then transferred into the glovebox with a nitrogen atmosphere. Afterward, either pristine $CH_3NH_3PbI_3$ thin film or the $CH_3NH_3PbI_3$:TiO_x BHJ composite thin film was prepared by one-step method rather than typical two-step method, *i.e.*, either pristine $CH_3NH_3PbI_3$ thin film or the $CH_3NH_3PbI_3$:TiO_X BHJ composite thin film was deposited on the top of PEDOT:PSS layer by spin-coat with a spin speed of 4000 RPM for 30 s from corresponding $CH_3NH_3PbI_3$ solution or $CH_3NH_3PbI_3$ mixed with TiO_X solution (with 5% and 10% by weight). After that, thin films were thermally annealed at 100 °C for 10 min and then cooled down to room temperature. Afterward, ~ 40 nm $PC_{61}BM$ thin film was spin-coated on the top of photoactive layer with a spin speed of 1500 rpm for 30 s. Finally, ~100 nm Al was thermally deposited on the top of $PC_{61}BM$ thin film in vacuum system with a base pressure of 10^{-6} Torr. The device area was measured to be 0.045 cm^2.

The current density *versus* voltage (*J–V*) characteristics of PSCs was tested by a Keithley model 2400 source measure unit. The light source was a Newport Air Mass 1.5 Global (AM1.5 G) full spectrum simulator with a light intensity of 100 mW/cm^2. The external quantum efficiency (EQE) spectrum was obtained on the solar cell quantum efficiency measurement system (QEX10). The scanning electron microscopy (SEM) images were got from a field emission scanning electron microscopy (Model JEOL-7401). Impedance spectroscopy was obtained on an HP 4194A impedance/gain-phase analyzer. Time-resolved photocurrent (TPC) measurement was done by the home-made set-up in our laboratory [23–26].

Schemes 1a and b display PHJ PSCs with a device configuration of ITO/PEDOT:PSS/$CH_3NH_3PbI_3$/$PC_{61}BM$/Al and BHJ PSCs with a device structure of ITO/PEDOT:PSS/$CH_3NH_3PbI_3$:TiO_X/$PC_{61}BM$/Al. It is clear that the only difference in PHJ PSCs and BHJ PSCs is the photoactive layer. In PHJ PSCs, the photoactive layer is pristine $CH_3NH_3PbI_3$ thin film, whereas, in BHJ PSCs, the photoactive layer is $CH_3NH_3PbI_3$:TiO_X thin film. Scheme 1c displays the highest occupied molecular orbit (HOMO) energy levels and the lowest unoccupied molecular orbit (LUMO) energy levels of $CH_3NH_3PbI_3$, TiO_X and $PC_{61}BM$, and the work functions of ITO, PEDOT:PSS and Al, respectively [5,19]. According to the band alignment, the introduction of TiO_X would decrease the energy barrier between $CH_3NH_3PbI_3$ thin film and the $PC_{61}BM$ EEL, which would benefit for electronsto be transported, resulting in an enhanced short-circuit current (J_{SC}) from BHJ PSCs as compared with that of PHJ PSCs. Thus, n-type TiO_X acts as the electron acceptors in BHJ PSCs, which is similar to that of BHJ organic solar cells [27].

The *J–V* characteristics of PHJ and BHJ PSCs under white light illumination with a light intensity of 100 mA/cm^2 are shown in Fig. 1a. The PHJ PSCs exhibit a J_{SC} of 18.83 mA/cm^2, an open-circuit voltage (V_{OC}) of 0.82 V, a fill factor (FF) of 74% and with a

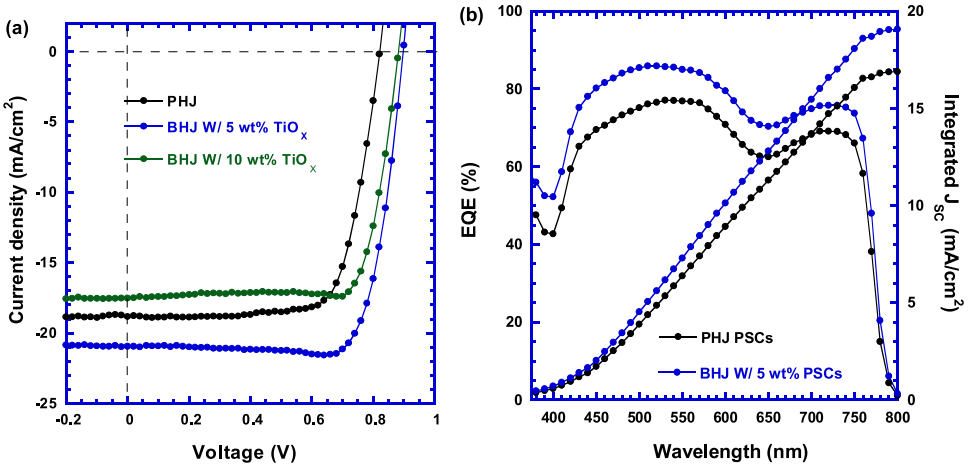

Fig. 1. (a) The *J–V* characteristics of PHJ PSCs by pristine $CH_3NH_3PbI_3$ thin film and BHJ PSCs by $CH_3NH_3PbI_3$ mixed with different ratios (5 wt% and 10 wt%) of TiO_X thin films. (b) The EQE spectra of PHJ PSCs by pristine $CH_3NH_3PbI_3$ thin film and BHJ PSCs by $CH_3NH_3PbI_3$ mixed with 5 wt% of TiO_X thin film.

Please cite this article in press as: T. Zhu, et al., Bulk heterojunction perovskite solar cells incorporated with solution-processed TiO_X nanoparticles as the electron acceptors, Chin. Chem. Lett. (2020), https://doi.org/10.1016/j.cclet.2020.02.004

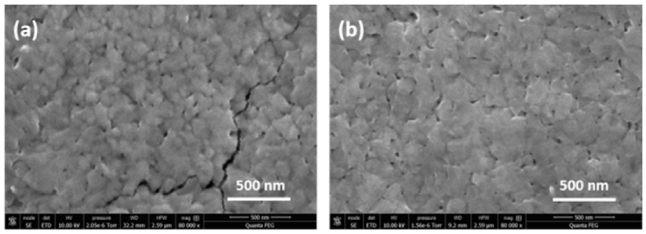

Fig. 2. Top-view SEM images of (a) pristine $CH_3NH_3PbI_3$ thin film and (b) $CH_3NH_3PbI_3$:TiO_X BHJ composite thin film.

corresponding PCE of 11.40%. All these device performance parameters are in good agreement with those reported values from PHJ PSCs, where $CH_3NH_3PbI_3$ thin film was processed by one-step method [28].The BHJ PSCs, where $CH_3NH_3PbI_3$ mixed with 5 wt % of TiO_X, show a J_{SC} of 20.93 mA/cm^2, a V_{OC} of 0.90 V, a FF of 80% and with a corresponding PCE of 14.91%, which is more than 30% enhancement as compared with that of PHJ PSCs. However, as the ratio of TiO_X is increased to 10 wt% in $CH_3NH_3PbI_3$:TiO_X thin film, the BHJ PSCs exhibit a J_{SC} of 17.52 mA/cm^2, a V_{OC} of 0.88 V, a FF of 80% and with a corresponding PCE of 12.28%, which show poor device performance. Such poor device performance is probably attributed to the crystallinity of perovskites is tuned by the excess TiO_X nanoparticles. The reproducibility of device performance is shown in Fig. S1 (Supporting information).

The EQE spectra of both PHJ PSCs and BHJ PSCs are shown in Fig. 1b. It is obvious that BHJ PSCs possess larger EQE values than those of PHJ PSCs from 380 nm to 800 nm. Based on the EQE spectra, the integrated photocurrent densities are 16.90 mA/cm^2 and 19.07 mA/cm^2 for PHJ PSCs and BHJ PSCs, respectively. The photocurrent densities obtained from the EQE spectra are consistent with J_{SC} values from the *J-V* characteristics (Fig. 1a). All these results demonstrate that TiO_x as the electron acceptors could facility separated electrons to be efficiently transported, resulting in boosted device performance of BHJ PSCs.

In order to understand the underlying enhanced device performance of BHJ PSCs, SEM is carried out to study film morphologies of pristine $CH_3NH_3PbI_3$ thin film and $CH_3NH_3PbI_3$:TiO_X BHJ composite thin film. Fig. 2 displays the top-view SEM images of pristine $CH_3NH_3PbI_3$ thin film and $CH_3NH_3PbI_3$:TiO_X BHJ thin film. Lots of pinholes and grain boundaries are presented in pristine $CH_3NH_3PbI_3$ thin film. As a result, PHJ PSCs exhibit poor device performance. On the contrast, a smoother and more

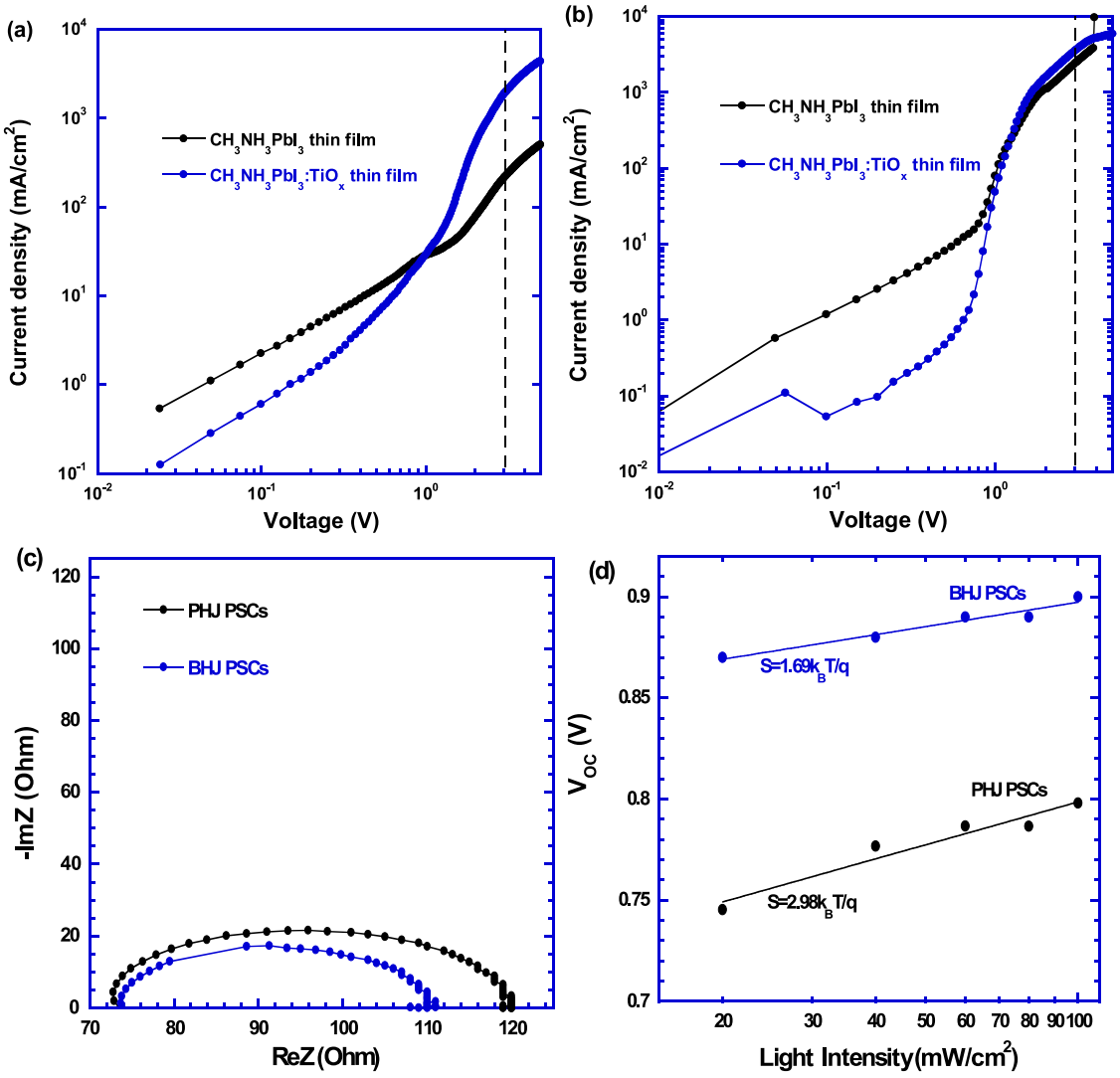

Fig. 3. The "log-log" plot of the *J-V* characteristics of (a) the electron-only diodes and (b) the hole-only diodes made by either pristine $CH_3NH_3PbI_3$thin film or $CH_3NH_3PbI_3$:TiO_x BHJ composites thin film. (c) The Nyquist plots of PHJ and BHJ perovskite solar cells measured under a one-sun illumination at an applied voltage of V_{OC}. (d) The light intensity dependence of V_{OC} for PHJ PSCs and BHJ PSCs.

Please cite this article in press as: T. Zhu, et al., Bulk heterojunction perovskite solar cells incorporated with solution-processed TiO_X nanoparticles as the electron acceptors, Chin. Chem. Lett. (2020), https://doi.org/10.1016/j.cclet.2020.02.004

compact surface is observed from $CH_3NH_3PbI_3$:TiO_X BHJ composite thin film, which indicates that the pinholes are probably filled with TiO_X nanoparticles. Furthermore, the grain size of $CH_3NH_3PbI_3$:TiO_X BHJ composite thin film is ~ 300 nm, which is significantly larger than that (~100 nm) of pristine $CH_3NH_3PbI_3$ thin film, reflecting that the introduction of TiO_X nanoparticles could tune the crystallization rate and promote the growth of larger perovskite crystals. Superior film morphology and large grain size would facility charge carriers to be transferred in $CH_3NH_3PbI_3$:TiO_X BHJ composite thin film. Therefore, as expected, BHJ PSCs exhibit enhanced device performance.

In order to investigate charge carrier transporting properties, charge carrier mobilities of pristine $CH_3NH_3PbI_3$ thin film and $CH_3NH_3PbI_3$:TiO_X BHJ composite thin film are studied based on space charge limited current (SCLC) method according to Mott-Gurney law [29–31]. The *J*–*V* characteristics of the electron-only diodes with a device structure of ITO/Al/active layer/$PC_{61}BM$/Al and the hole-only diodes with a device structure of ITO/PEDOT:PSS/active layer/MoO_X/Ag, where active layer is either pristine $CH_3NH_3PbI_3$ thin film or $CH_3NH_3PbI_3$:TiO_X BHJ composite thin film, are shown in Figs. 3a and b. At a low voltage, the *J*–*V* curves are in the ohmic region, which indicates that the current is followed the Ohm's law. In the trap-filling region, the SCLC is dominated and which is described by $J = \frac{8}{9}\varepsilon_0\varepsilon\mu\frac{V^2}{L^3}$ [31], where J is the current density, ε_0 is the permittivity of free space (8.85×10^{-12} CV^{-1} m^{-1}), ε is the relative dielectric constant of active material, μ is the mobility of charge carrier, *V* is the applied voltage and *L* is the thickness of active layer.In our study, the value of ε is 32 for $CH_3NH_3PbI_3$ [20,32] and the film thickness of $CH_3NH_3PbI_3$ is ~ 300 nm, which was measured by DektakXT surface profile meter. For pristine $CH_3NH_3PbI_3$ thin film, the hole mobility is measured to be 2.19×10^{-3} cm^2 V^{-1} s^{-1}), which is ten times higher than the electron mobility of 2.03×10^{-4} cm^2 V^{-1} s^{-1}. The charge carrier mobilities of pristine $CH_3NH_3PbI_3$ thin film are consistent with reported values [32,33]. The hole mobility larger than the electron mobility indicates that charge carrier transporting within pristine $CH_3NH_3PbI_3$ thin film was unbalanced. For $CH_3NH_3PbI_3$:TiO_X BHJ composite thin film, the hole mobility is measured to be 3.47×10^{-3} cm^2 V^{-1} s^{-1}, which is nearly the same as the electron mobility (1.84×10^{-3} cm^2 V^{-1} s^{-1}, which is about ten times larger than that (2.03×10^{-4} cm^2 V^{-1} s^{-1}) of pristine $CH_3NH_3PbI_3$ thin film. These results not only demonstrate that the electron mobility of $CH_3NH_3PbI_3$ thin film is tuned by the TiO_X electron acceptors, but also indicate that charge carrier transporting within $CH_3NH_3PbI_3$:TiO_X BHJ composite thin film is more balanced than those of pristine $CH_3NH_3PbI_3$ thin film. As a result, BHJ PSCs by $CH_3NH_3PbI_3$:TiO_X BHJ composite thin film exhibit boosted J_{SC}

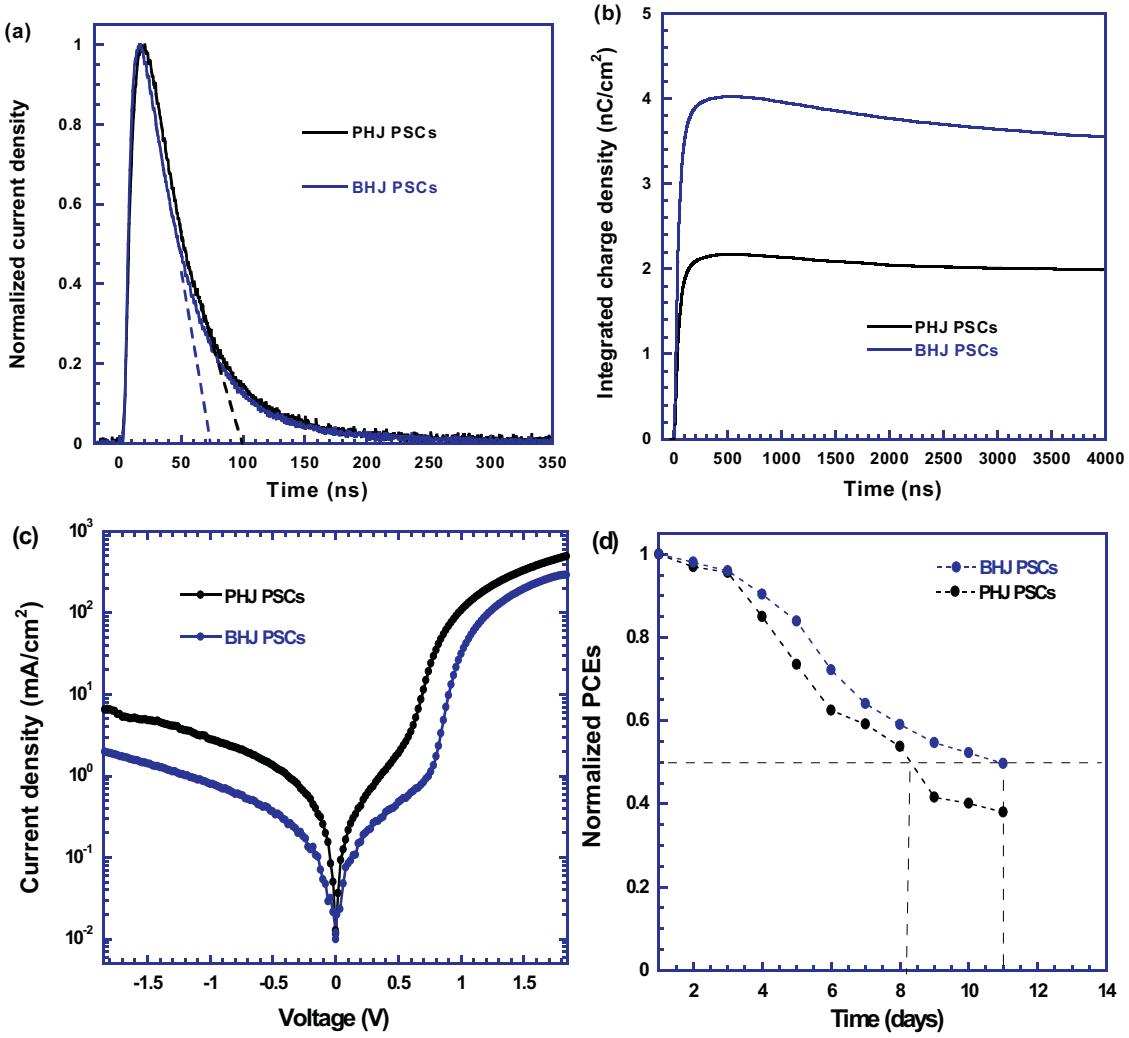

Fig. 4. (a) The normalized TPC curves and (b) the integrated charge density curves of PHJ PSCs and BHJ PSCs, under bias of −1 V. (c) The *J*-*V* characteristics of both PHJ PSCs and BHJ PSCs measured in dark. (d) The self-stabilities of PHJ PSCs and BHJ PSCs.

Please cite this article in press as: T. Zhu, et al., Bulk heterojunction perovskite solar cells incorporated with solution-processed TiO_X nanoparticles as the electron acceptors, Chin. Chem. Lett. (2020), https://doi.org/10.1016/j.cclet.2020.02.004

To further understand the underlying of enlarged J_{SC} from BHJ PSCs, impedance spectroscopy (IS) is applied to investigate the electric properties of both PHJ PSCs and BHJ PSCs. In the IS spectra, the series resistance (R_S) of PSCs is the sum of the electrodes' sheet resistance (R_{sheet}) and the internal charge transfer resistance (R_{CT}) [18,25,34,35]. Nyquist plots of both PHJ and BHJ PSCs under a one-sun illumination at the voltage of V_{OC} are shown in Fig. 3c. The R_{CT} of PHJ PSCs is ~46 Ω, whereas, the R_{CT} of BHJ PSCs is ~ 36 Ω. The smaller R_{CT}, the larger J_{SC} [18]. Thus, BHJ PSCs exhibit a larger J_{SC} than that of PHJ PSCs.

The light intensity dependence of V_{OC} is further studied for investigation of charge carrier recombination in both PHJ PSCs and BHJ PSCs. As shown in Fig. 3d, both PHJ PSCs and BHJ PSCs follow the relationship $V_{OC} \propto S\ln(I)$ [36,37], where S is the slope and I is the light intensity. For PHJ PSCs, $S = 2.98k_BT/q$, where k_B is the Boltzmann constant, q is the elementary charge and T is the room temperature in Kelvin, whereas, for BHJ PSCs, S = $1.69k_BT/q$. It was reported that a smaller S reflects that less trap-assisted charge recombination happens in PSCs. Thus, BHJ PSCs possess less trap-assisted charge recombination, consequently higher J_{SC} compared to that of PHJ PSCs.

The transient photocurrent (TPC) measurement is further carried out to investigate the difference in charge extraction times between PHJ PSCs and BHJ PSCs. Fig. 4ashowsthe normalized TPC curves of PHJ PSCs and BHJ PSCs under −1 V bias, in which the charge carrier recombination process would be suppressed, and all the photocurrent is related to the charge extraction process. The charge extraction times for PHJ PSCs and BHJ PSCs are ~ 100 ns and ~ 75 ns, respectively. A shorter charge extraction time indicates that separated charge carriers are efficiently collected by the electrodes in BHJ PSCs. The integrated charge densities versus times for both PHJ PSCs and BHJ PSCs are shown in Fig. 4b. It is obvious that the total extraction charge densities of BHJ PSCs are much larger than those of PHJ PSCs, indicating that more charge carriers are generated by BHJ PSCs rather than PHJ PSCs. All these results demonstrate that BHJ PSCs possess higher J_{SC} as compared with that of PHJ PSCs.

To understand larger V_{OC} observed from BHJ PSCs, the *J-V* characteristics of both PHJ and BHJ PSCs measured in dark are conducted and the results are shown in Fig. 4c. It is clear that BHJ PSCs possess lower dark current densities than those of PHJ PSCs under reverse biases. Based on the electronic properties of two-term diodes, the V_{OC} is described as $V_{OC} = \frac{nk_BT}{q}\ln(\frac{J_{ph}}{J_0} + 1)$ [31,38], where q is the elementary electron charge, k_B is the Boltzmann's constant, T is the temperature, n is the ideality factor, J_0 is the reverse dark current density, J_{ph} is the photocurrent, respectively. Thus, lower dark current densities observed from BHJ PSCs indicate that BHJ PSCs exhibit larger V_{OC} compared to that of PHJ PSCs.

In addition, the self-stabilities of PHJ PSCs and BHJ PSCs are primarily studied. Fig. 4d presents normalized PCEs of both PHJ PSCs and BHJ PSCs versus the time. It is found that the trends of decay in PCEs for both PHJ PSCs and BHJ PSCs are almost the same. However, BHJ PSCs still maintain about 50% PCEs of its original value after nearly 12 days while PHJ PSCs remain less than 50% PCEs of its original value only 8 days. These primary results indicate that BHJ PSCs possess good stability compared to that of PHJ PSCs. Such elongated stability is partially due to the superior film morphology of $CH_3NH_3PbI_3$:TiO_X BHJ composite thin film.

In conclusion, we reported high-performance bulk heterojunction perovskite solar cells, where $CH_3NH_3PbI_3$ is blended with solution-processed n-type TiO_x nanoparticle as the photoactive layer to balance charge carrier transporting properties for addressing the intrinsic electronic properties of perovskite materials. We found that the $CH_3NH_3PbI_3$:TiO_x bulk heterojunction thin film possesses enhanced and balanced charge carrier mobilities, superior film morphology with enlarged crystal sizes. Moreover, bulk heterojunction perovskite solar cells possess suppressed trap-induced charge recombination as compared with that of planar heterojunction perovskite solar cells. Thus, bulk heterojunction perovskite solar cells by $CH_3NH_3PbI_3$ mixed with 5 wt% of TiO_X show superior photovoltaic performance and better stability over planar heterojunction perovskite solar cells. All these results demonstrate that perovskite solar cells with a bulk heterojunction device structure are one of the facile approaches to boost device performance.

Declaration of competing interest

The authors declare that they have no known competing financial interests or personal relationships that could have appeared to influence the work reported in this paper.

Acknowledgments

The authors at The University of Akron acknowledge Air Force Scientific Research Program (No. FA9550-15-1-0292) and National Science Foundation (Nos. EECs 1,351,785 and EECs 1,903,303) for financial support.

Appendix A. Supplementary data

Supplementary material related to this article can be found, in the online version, at doi:https://doi.org/10.1016/j.cclet.2020.02.004.

References

[1] A. Kojima, K. Teshima, Y. Shirai, T. Miyasaka, J. Am. Chem. Soc. 131 (2009) 6050.
[2] L. Chu, W. Ahmad, W. Liu, et al., Nano-Micro Lett. 11 (2019) 16.
[3] L. Chu, W. Liu, Z.F. Qin, et al., Sol. Energy Mater. Sol. Cells 178 (2018) 164–169.
[4] S.D. Stranks, H.J. Snaith, Nat. Nanotechnol. 10 (2015) 391–402.
[5] C.C. Chueh, C.Z. Li, A.K.Y. Jen, Energy Environ. Sci. 8 (2015) 1160–1189.
[6] https://www.nrel.gov/pv/assets/pdfs/best-research-cell-efficiencies.20190802.pdf.
[7] E. Edri, S. Kirmayer, S. Mukhopadhyay, et al., Nat. Commun. 5 (2014) 3461.
[8] Z.Z. Xu, X. Yin, Y.J. Guo, Y. Pu, M. He, J. Mater, Chem. C 6 (2018) 4746–4752.
[9] H. Wang, R. Jiang, M.L. Sun, et al., J. Mater. Chem. C 7 (2019) 1948–1954.
[10] W.L. Lu, R. Jiang, X. Yin, L.Y. Wang, Nano Res. 12 (2019) 159–163.
[11] L. Chu, J. Zhang, W. Liu, et al., ACS Sustain. Chem. Eng. 6 (2018) 5588–5597.
[12] R. Lindblad, D. Bi, B.W. Park, et al., J. Phys. Chem. Lett. 5 (2014) 648–653.
[13] M.M. Lee, J. Teuscher, T. Miyasaka, T.N. Murakami, H.J. Snaith, Science 338 (2012) 643–647.
[14] Y.J. Jeon, S. Lee, R. Kang, et al., Sci. Rep. 4 (2014) 6953.
[15] K. Wang, C. Liu, P.C. Du, J. Zheng, X. Gong, Energy Environ. Sci. 8 (2015) 1245–1255.
[16] C.H. Chiang, C.G. Wu, Nat. Photonics 10 (2016) 196.
[17] W. Xu, L. Zheng, T. Zhu, L. Liu, X. Gong, ACS Appl. Mater. Interfaces 11 (2019) 34020–34029.
[18] C. Liu, K. Wang, P.C. Du, et al., Adv. Energy Mater. 5 (2015)1402024.
[19] C. Liu, K. Wang, P.C. Du, et al., ACS Appl. Mater. Interfaces 7 (2015) 1153–1159.
[20] W.Z. Xu, L.Y. Zheng, X.T. Zhang, et al., Adv. Energy Mater. 8 (2018) 1703178.
[21] E. Edri, S. Kirmayer, A. Henning, et al., Nano Lett. 14 (2014) 1000–1004.
[22] K. Wang, C. Liu, P.C. Du, H.L. Zhang, X. Gong, Small 11 (2015) 3369–3376.
[23] J. Seifter, Y.M. Sun, A.J. Heeger, Adv. Mater. 26 (2014) 2486–2493.
[24] L. Zheng, S. Mukherjee, K. Wang, et al., J. Mater. Chem. A 5 (2017) 23831–23839.
[25] K. Wang, L. Zheng, T. Zhu, et al., Nano Energy 67 (2020)104229.
[26] T. Zhu, L. Zheng, Z. Xiao, et al., Sol. Rrl 3 (2019)1900322.
[27] G. Yu, J. Gao, J.C. Hummelen, F. Wudl, A.J. Heeger, Science 270 (1995) 1789–1791.
[28] S. Pang, D. Chen, Emerging Solar Energy Mater. (2018) 217.
[29] S. Takeshita, All Theses (2008) 473.
[30] A. Rose, Phys. Rev. 97 (1955) 1538–1544.
[31] S.A. Moiz, I.A. Khan, W.A. Younis, K.S. Karimov, Conduct. Polym. (2016) 91.
[32] Q. Dong, Y. Fang, Y. Shao, et al., Science 347 (2015) 967–970.
[33] R.L. Milot, G.E. Eperon, H.J. Snaith, M.B. Johnston, L.M. Herz, Adv. Funct. Mater. 25 (2015) 6218–6227.
[34] X. Yin, Y.J. Guo, Z.S. Xue, et al., Nano Res. 8 (2015) 1997–2003.
[35] V. Gonzalez-Pedro, E.J. Juarez-Perez, W.S. Arsyad, et al., Nano Lett. 14 (2014) 888–893.
[36] S.R. Cowan, A. Roy, A.J. Heeger, Phys. Rev. B 82 (2010) 245207.
[37] S.R. Cowan, N. Banerji, W.L. Leong, A.J. Heeger, Adv. Funct. Mater. 22 (2012) 1116–1128.
[38] G. Wetzelaer, M. Kuik, M. Lenes, P. Blom, Appl. Phys. Lett. 99 (2011)153506.

Please cite this article in press as: T. Zhu, et al., Bulk heterojunction perovskite solar cells incorporated with solution-processed TiO_X nanoparticles as the electron acceptors, Chin. Chem. Lett. (2020), https://doi.org/10.1016/j.cclet.2020.02.004